Materials Transactions, Vol. 60, No. 8 (2019) pp. 1489 to 1499
Special Issue on Severe Plastic Deformation for Nanomaterials with Advanced Functionality
©2019 The Japan Institute of Metals and Materials

Phase Transformations Induced by Severe Plastic Deformation

Andrey Mazilkin[1,3], Boris Straumal[1,2,3,4,*], Askar Kilmametov[2,3], Petr Straumal[4] and Brigitte Baretzky[3]

[1]*Institute of Solid State Physics, Russian Academy of Sciences, 142432 Chernogolovka, Russia*
[2]*Chernogolovka Scientific Center of Russian Academy of Sciences, 142432 Chernogolovka, Russia*
[3]*Karlsruhe Institute of Technology (KIT), Institute of Nanotechnology, 76344 Eggenstein-Leopoldshafen, Germany*
[4]*National University of Science and Technology (MISIS), 119049 Moscow, Russia*

Severe plastic deformation (SPD) can induce various phase transformations. After a certain strain, the dynamic equilibrium establishes between defects production by an external force and their relaxation (annihilation). The grain size, hardness, phase composition etc. in this steady-state does not depend on the initial state of a material and is, therefore, equifinal. In this review we discuss the competition between precipitation and dissolution of precipitates, amorphization and (nano)crystallization, SPD-induced accelerated mass-transfer, allotropic and martensitic transitions and formation of grain boundary phases. [doi:10.2320/matertrans.MF201938]

(Received March 1, 2019; Accepted May 15, 2019; Published June 28, 2019)

Keywords: *severe plastic deformation, phase transformations, thermodynamics, kinetics*

1. Introduction

Severe plastic deformation (SPD) is a novel class of mechanical treatment which permits to apply a very high strain to the material without its failure, which is not possible with traditional methods. SPD always leads to strong grain refinement or even to amorphization of a material. At the same time, SPD can drive the phase transformations.[1–6] In other words the phases in a material before and after SPD can be different. Frequently, after SPD a material contains such phases as if it was annealed at elevated temperature and then quickly quenched.[3] Thus, SPD opens completely new ways for tailoring microstructure and properties of materials. The understanding of SPD-driven phase transformations is the topic of this review.

2. Steady-State during SPD

The important feature of SPD is that the sample cannot break during straining, and its shape remains more or less unchanged. It is especially well pronounced in case of high pressure torsion (HPT). The small disk between two anvils conserves its shape independently on number of anvil rotations. The torsion can continue until the anvils (typically made of WC-Co alloy) break. For example, in case of HPT of Nd–Fe–B alloys the anvils withstand only about 20 rotations[7,8] but in case of soft aluminium-, magnesium- or copper-based alloys HPT can continue up to hundreds or even thousands anvil rotations.[9–13] When the straining starts, the amount of lattice defects (like vacancies, dislocations, grain boundaries) expectedly increases. However, it would be strange to anticipate that the number of defects would increase infinitely during endless anvil rotations. Even when the HPT proceeds at room temperature when the coefficients of bulk diffusion are below 10^{-30}–10^{-40} m^2/s, the relaxation starts. Its rate increases with increasing concentration of defects until the dynamic equilibrium establishes. In other words, the rate of defects production becomes equal to the rate of their annihilation (relaxation). Here it is appropriate to mention that usually HPT (and generally SPD) takes place at room temperature and the samples are almost not heated during HPT.[14,15] After HPT treatment they are usually just a little bit warm. The direct temperature measurements between anvils witness that the temperature during SPD does not exceed about 40°C.[16,17]

Thus, after a certain number of anvil rotations, the rate of defects production becomes equal to the rate of their annihilation (relaxation) and the steady-state is reached.[5,18] The easiest way to observe it is to measure the torsion torque during HPT. It increases during the transient stage, but quickly saturates after 1–1.5 rotations in case of Al-, Cu-, Mg- or even Ti-based alloys.[1,5,13,16,19] In case of harder alloys like Nd–Fe–B the torsion torque saturates after 2–2.5 anvil rotations.[5,7,8] Not only torsion torque, but also the values of the properties or structural parameters saturate in the steady state. For example, the most prominent feature of SPD is the grain refinement.[13,20–25] If one starts to deform the material with grain size of several millimetres, it quickly decreases down to few hundreds of nanometers. Then, the grain size reach the steady-state value, stabilises and does not decrease anymore.[17,26–29] In the same material, the steady-state grain size depends first of all on the SPD mode. For example, the smallest grain size in copper and copper-based alloys of about 15 nm is reached by the ball milling (Fig. 1).[30] The second strongest grain refiner is HPT.[1,31–36] This is followed by planar twist channel angular extrusion (PTCAE),[37] equal channel angular pressing (ECAP),[34,38] equal channel angular pressing with the subsequent HPT (ECAP+HPT),[34] equal channel angular pressing with following cold rolling (ECAP + CR),[39] simple shear extrusion (SSE),[40,41] and constrained groove pressing (CGP).[42] Same tendency is true also for aluminium and its alloys.[43] The steady-state grain size is also the function of HPT pressure, strain rate and temperature.[5,18] It decreases with increasing melting temperature, atomic bond energy, specific heat capacity and activation energy for self-diffusion.[18,44] One has to underline that the grain size in the dynamic equilibrium is a real steady-state value. It means that it is reached not only "from the top" but also "from the bottom". In other words, if one starts HPT of steel from the

*Corresponding author, E-mail: straumal@issp.ac.ru

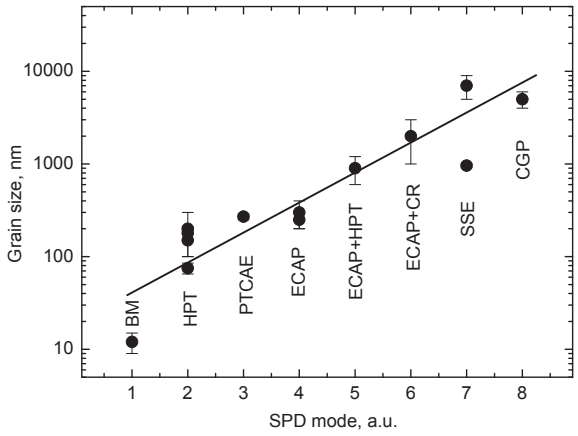

Fig. 1 Steady-state grain size in copper subjected to the different SPD modes: 1 – Ball milling (BM),[30] 2 – High pressure torsion (HPT),[1,31–36] 3 – Planar twist channel angular extrusion (PTCAE),[37] 4 – Equal channel angular pressing (ECAP),[34,38] 5 – ECAP+HPT,[34] 6 – Equal channel angular pressing with following cold rolling (ECAP + CR),[39] 7 – Simple shear extrusion (SSE),[40,41] 8 – Constrained groove pressing (CGP).[42]

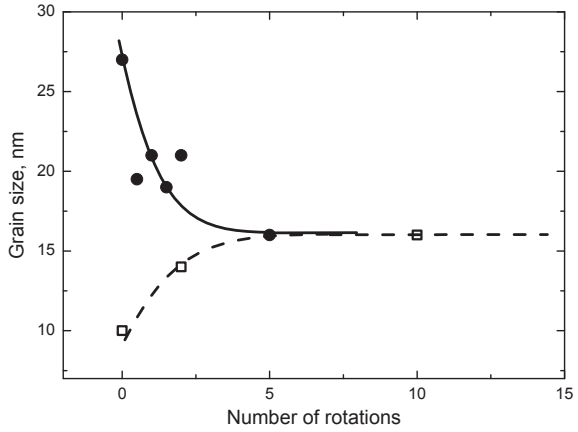

Fig. 2 Grain size plotted vs. number of torsions for pure coarse-grained steel sample (filled circles)[46] and nanocrystalline steel produced by mechanical alloying (open squares).[9]

coarse-grained sample, one quickly reaches the grain size of 15–20 nm[28,45–51] (Fig. 2). However, if one starts to deform the nanocrystalline steel sample with grain size of 10 nm produced by mechanical alloying, the grains do not become smaller. To the contrary, they grow during SPD up to the same steady-state value of 15–20 nm (Fig. 2).[9] Similar phenomenon was observed also in nickel[52,53] and copper.[54]

Together with observation of grain refinement, a huge amount of experimental data is collected on the Vickers microhardness during and after SPD of copper, aluminium, titanium, magnesium alloys, steels etc.[10,17,29,55–67] Usually microhardness increases during SPD.[10,17,29,55–67] It correlates also with tensile strength.[13,24,25,57,60,68–70] It is true not only for rotation angle for HPT but also for number of passes during equal channel angular pressing (ECAP).[62] The main mechanism here is the Hall-Petch hardening due to the grain refinement.[71] Few exclusions only support this fact. For example, in Al–Zn alloys the Hall-Petch hardening competes with softening driven by the decomposition of (Al) solid solution, and after HPT the alloy is softer than before HPT (Fig. 3).[31,56,72,73] Similar to the grain size, the hardness

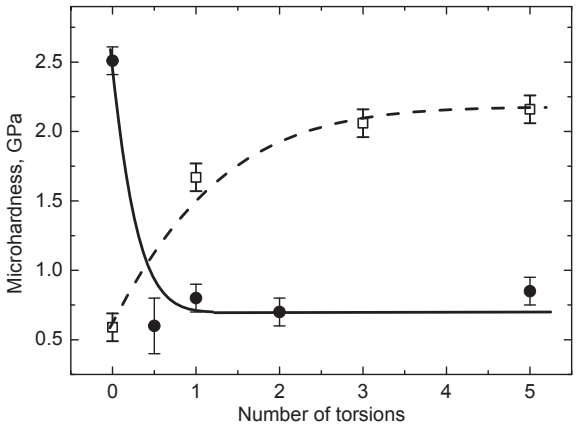

Fig. 3 Vickers microhardness plotted vs. number of torsions for pure Al–30 wt.% Zn (filled circles)[31] and Al–8.8 wt.% Mg alloys (open squares).[55]

value is also a function of material and SPD mode. So, if to increase the purity of aluminium, one observes the transition from hardening to softening during HPT.[74] Thus, when the initial hardness of an alloy is higher than the steady-state one, then softening rather than hardening is observed during SPD.[72]

The decrease of grain size and increase of Vickers microhardness after HPT, ECAP and alternating roll bonding (ARB) correlates with increase of electrical resistivity of copper.[62] It is important to underline that different properties (grain size, hardness, torsion torque, lattice parameter, resistivity etc.) reach steady state not at the same time.

3. Competition between Dissolution of Precipitates and Decomposition of Supersaturated Solid Solution

It has been long time generally believed that SPD always leads to the grain refinement[23,75] and to the dissolution of precipitates and formation of supersaturated solid solution. However, we demonstrated above that the grain size decreased during SPD only in the case if the grains in the initial sample before SPD are larger than those in the steady-state. If the grains before SPD are smaller than in the steady state, they will grow during the deformation and reach the same steady-state grain size "from below" (see Fig. 2). This is true also for the SPD-induced hardening/softening (see Fig. 3). Similar is the situation with dissolution/precipitation process. In the steady-state during SPD a certain concentration in the solid solution c_{ss} establishes. Its value is controlled by the dynamic equilibrium between competing dissolution and precipitation. If the initial concentration in a solid solution c_{init} is below c_{ss}, it increases during SPD and precipitates dissolve. Otherwise, if $c_{init} > c_{ss}$, the concentration of second component in a solid solution decreases and new precipitates appear (so-called dynamic ageing). For the first time such dynamic ageing has been observed in Al–Zn alloys.[73] Now it is an established topic for investigations and the instrument for the tailoring the properties of materials.[76] Below, the decomposition of the solid solution in all discussed cases leads to the formation of small particles of the second phase (i.e. to precipitation). Therefore, for this

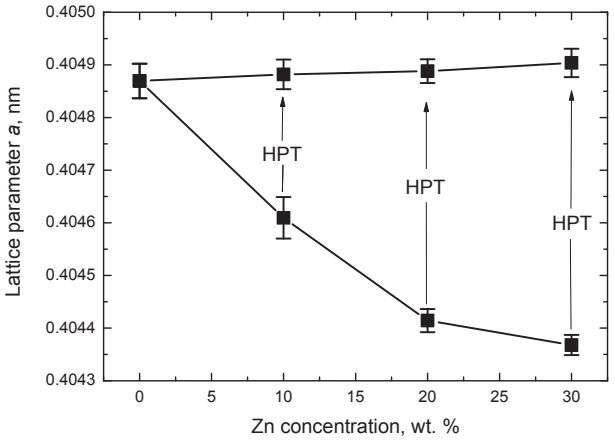

Fig. 4 Dependence of the lattice parameter in aluminium matrix on the total zinc concentration in the Al–Zn alloys before and after HPT.[73)]

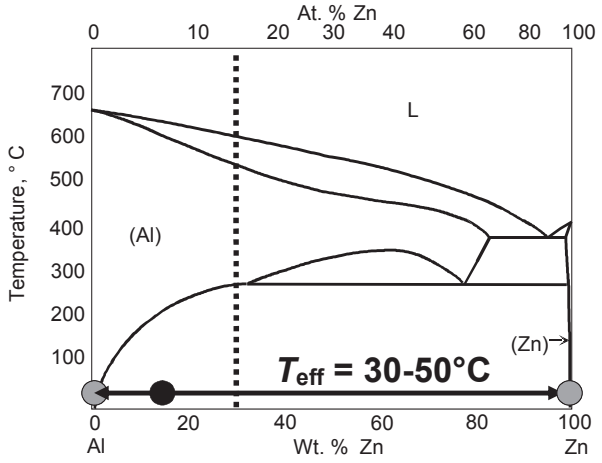

Fig. 5 Al–Zn phase diagram. Vertical dotted line shows the composition of Al–30 wt.% Zn alloy. Large black circle shows the composition of supersaturated (Al) solid solution in coarse-grained Al–30 wt.% Zn alloy before HPT (it contained 15 wt.% Zn). Large grey circles show the composition of phases in ultra-fine-grained Al–30 wt.% Zn alloy after HPT.[73)] The value of $T_{eff} = 30–50°C$ is also given.

discussion we use the terms "decomposition" and "precipitation" as synonyms.

The as-cast Al–Zn alloys were subjected to HPT at 5 turns, 5 GPa and 1 rpm.[73)] The coarse-grained supersaturated solid solution (Al) in the as-cast Al–30 wt.% Zn alloy contained about 15 wt.% Zn. Zn concentration in the solid solution for Al–20 wt.% Zn and Al–10 wt.% Zn alloys (measured locally by the electron-probe microanalysis) was 7 and 3 wt.% Zn, correspondingly. In Fig. 4 the respective values for the lattice parameter in (Al) are given, they are well below the lattice parameter in pure aluminium. The HPT at room temperature produced nanograined pure Al and pure Zn particles.[20,73)] The supersaturated solid solution also completely decomposed, and the lattice parameter in all three alloys became non-distinguishable from that of pure aluminium (Fig. 4). The composition of the solid solutions in Al–30 wt.% Zn before and after the HPT is shown by black and grey circles in Fig. 5 correspondingly. The decomposition during SPD proceeds extremely quickly. Already after about 0.5 rotations of anvils the lattice spacing becomes equal to that of Al and microhardness reaches its steady-state value.[73)]

The competition between dissolution of precipitates and decomposition of supersaturated solid solution has been studied in details for the binary copper alloys.[6)] Physically, it is the steady-state concentration in the solid solution c_{ss} which establishes during SPD. However, in order to compare different binary alloys with different maximal solubilities of a second component, an idea of a so-called effective temperature T_{eff} is very useful. Thus, after SPD the concentration c_{ss} of a second component in the matrix solid solution is as high as if the sample has been annealed at a certain (elevated) temperature T_{eff}. In other words, c_{ss} is equal to the solubility of a second component at T_{eff}. The solubility is defined by the solvus line in the equilibrium binary phase diagram.

Consider the example of competition between dissolution and precipitation in Cu–Co system.[32,77,78)] The as cast Cu–4.9 wt.% Co alloy contained grains of Cu-based solid solution (with grain size 10–20 μm), Co particles with size about 2 μm and fine dispersed Co precipitates with a size about 10–20 nm.[32,77,78)] Cobalt fully dissolved in copper matrix after annealing at 1060°C for 10 h (sample 2). The grain size after this annealing was about 50 μm. During annealing at 570°C for 840 h (sample 1), the Cu-based solid solution almost fully decomposed: less than 0.5 wt.% Co remained dissolved in Cu (based on XRD measurements and phase diagram[29)]).

After HPT of both samples the Cu grain size drastically decreased to about 200 nm, and that of Co-precipitates to only 10–20 nm (insets in Fig. 6). The lattice parameter of Sample 1 before deformation is very close to that of pure copper (diamond in Fig. 6). With an increasing number of rotations, the lattice parameter of Sample 1 decreased and that of Sample 2 increased. After 5 anvil rotations (1800 deg.) the lattice parameter in both samples becomes almost undistinguishable and corresponds to the solid solution of Co in Cu with nearly 2.5 wt.%. In other words, the composition of the solid solution in the Cu–4.9 wt.% Co alloy after HPT does not depend on the initial state prior to HPT. This is a so-called *equifinal composition* $c_{eq} \approx 2.5$ wt.% Co. Thus, the steady-state with respect to the grain size, size of Co precipitates, torsion torque and concentration of Co in a solid solution during HPT is indeed *equifinal*. The composition of Cu-rich matrix in both alloys before and after HPT is shown in the Cu–Co phase diagram (Fig. 7). The solid solution in samples 1 and 2 after HPT contains as much Co $c_{eq} \approx 2.5$ wt.% Co, as if they would be annealed at $T_{eff1} = 920 \pm 30$°C and $T_{eff2} = 870 \pm 30$°C, respectively.

Here the analogy appears between thermodynamic *equilibrium* when the composition of phases does not depend on the starting state and *equifinality* when the composition of phases in a steady-state during SPD also does not depend on the phases in a starting state. The values like equivalent (effective) temperature T_{eff} and steady-state (equifinal) composition of solid solution c_{eq} are frequently called attractors in the thermodynamics of non-equilibrium (or open) systems.[79)]

In Ref. 6) the values of T_{eff} were compared for several Cu-based alloys Cu–Ni,[80)] Cu–Co,[32,77,78)] Cu–Sn,[81–83)] Cu–In,[84,85)] Cu–Cr,[86)] Cu–Ag,[87–89)] Cu–Al–Ni[90,91)] Cu–Hf[6)] (Fig. 8). The T_{eff} linearly increases with increase of activation

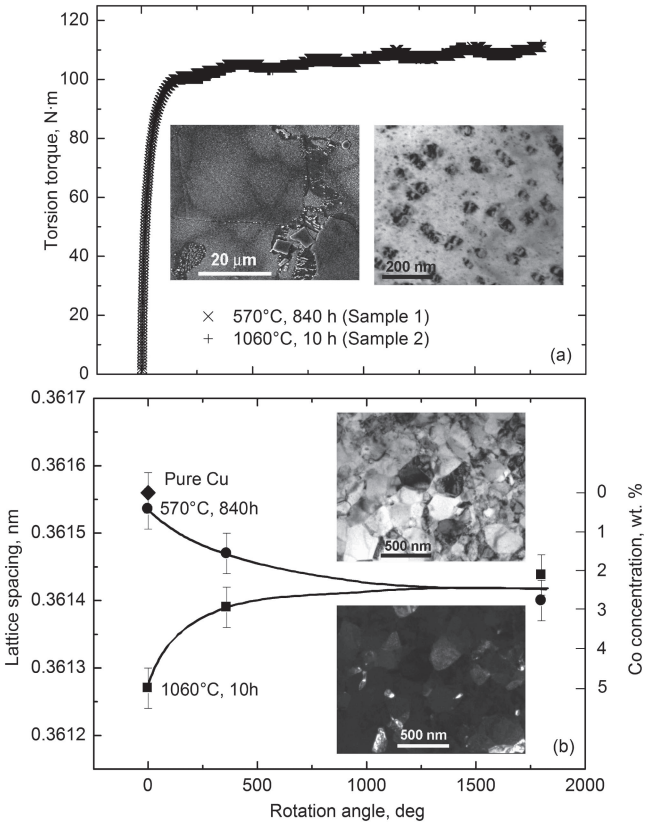

Fig. 6 (a) Dependence of torsion torque on the rotation angle. Insets: SEM (left) and bright-field TEM (right) micrographs of Cu–4.9 wt.% Co alloy after annealing at 570°C for 840 h. (b) Dependence of lattice spacing on the rotation angle. Circles mark the lattice spacing in Sample 1 annealed at 570°C for 840 h. Squares correspond to the Sample 2 annealed at 1060°C for 10 h. Diamond shows the lattice spacing for pure copper. The respective Co concentration is shown on the right vertical axis, $c_{eq} \approx$ 2.5 wt.% Co. Insets: Bright-field (top) and dark-field (bottom) TEM micrographs of Cu–4.9 wt.% Co alloy after annealing at 570°C for 840 h and HPT (6 GPa, 5 rot, 1 rpm).[32]

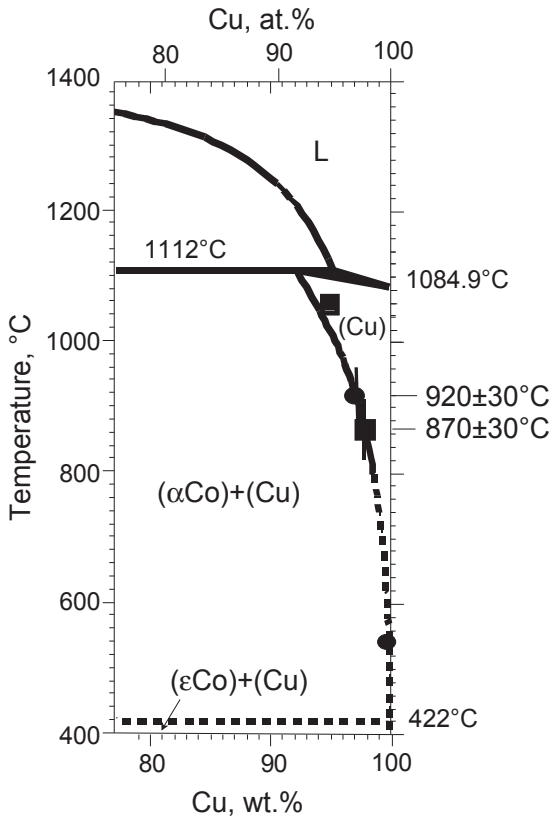

Fig. 7 The Cu-rich part of the Co–Cu phase diagram.[29] The composition of Cu-rich matrix in both alloys before and after HPT is shown. Circles mark the data for Sample 1 annealed before HPT at 570°C. Squares correspond to the Sample 2 annealed before HPT at 1060°C.[31] Steady-state (equifinal) composition of solid solution c_{eq} is about 2.5 wt.% C.[32]

enthalpy of bulk tracer diffusion H_D. The correlation between activation enthalpy of bulk tracer diffusion H_D and melting temperature T_m of diffusing alloying component also has been found. As a result, T_{eff} linearly increases with increase of melting temperature T_m of diffusing alloying component as well. The observed correlations allow one to predict the behaviour and phase transitions in the Cu-based alloys under high pressure torsion.

4. Amorphization and Nanocrystalisation

SPD produces high amount of defects, thus the material is very far from equilibrium during SPD. Nevertheless, one can *use the equilibrium phase diagrams* as an instrument for the

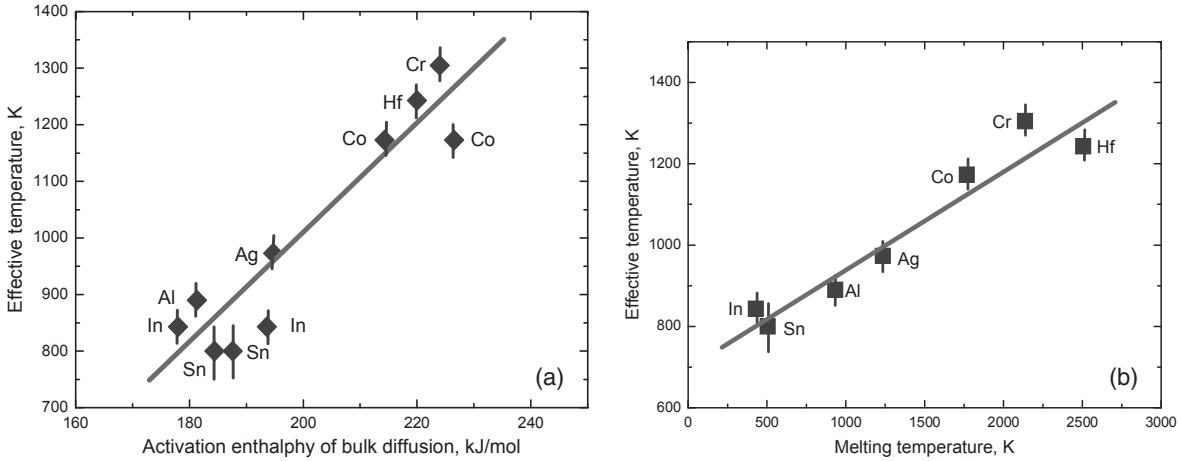

Fig. 8 (a) Dependence between effective temperature of HPT treatment T_{eff} of copper-based solid solutions and activation enthalpy of bulk tracer diffusion H_D of alloying element.[6] (b) Correlation between effective temperature T_{eff} and melting temperature T_m of alloying element in various Cu-based alloys.

description of *phase transformations in the non-equilibrium conditions*. This idea goes back to the work of Georges Martin who developed it for the description of phase transformations under strong irradiation.[92] His main idea was that the forced mixing induced by irradiation emulates the increase of entropy and changes the thermodynamic potentials in the alloy. The equilibrium configuration of the solid under irradiation flux φ at temperature T is identical to the configuration at $\varphi = 0$ and a certain effective temperature T_{eff}:

$$T_{\text{eff}} = T(1 + \Delta). \quad (1)$$

If the irradiation-driven movements of atoms are similar in amplitude to conventional diffusion jumps, they can be described by the "ballistic" diffusion coefficient D_{ball} and $\Delta = D_{\text{ball}}/D_{\text{b}}$, where D_{b} is conventional bulk diffusion coefficient, possibly increased due to the non-equilibrium defect concentration.[92] It means that one can use the equilibrium phase diagram for the description of the system under irradiation, but at T_{eff} instead of the actual temperature T. For example, if the liquid phase is present in the phase diagram at T_{eff}, the amorphous phase would appear under irradiation.[92] Thus, G. Martin proposed to find a temperature T_{eff} (usually called effective temperature) in an equilibrium phase diagram where the given phase appears under irradiation. The composition of phases after SPD allows to localize those phases in the respective equilibrium phase diagram and to estimate the effective temperature T_{eff}. Such a schematic diagram is shown in Fig. 9. We already used this idea for description of the SPD influence (see Section 3). In our case we use the value of D_{HPT} for the diffusion-like mass-transfer induced by HPT instead of D_{ball}.

The obvious example for the T_{eff} approach is the amorphization. Let us consider first the HPT of Nb–Ni–Y alloys.[93,94] The coarse-grained as-cast Ni–20 wt.% Nb–30 wt.% Y and Ni–18 wt.% Nb–22 wt.% Y alloys contained before high pressure torsion (HPT) the NiY, $NbNi_3$, Ni_2Y, Ni_7Y_2 and Ni_3Y phases (point *g*, Fig. 9) (Fig. 10(a)).[95,96] After HPT these alloys transformed into a mixture of two nanocrystalline NiY and $Nb_{15}Ni_2$ phases and two different amorphous phases (one was Y-rich and another Nb-rich) (point 6, Fig. 9). The Ni–Nb–Y phase diagram contains two immiscible melts above 1440°C (Fig. 10(a)).[96] Therefore, the effective temperature is slightly above $T_{\text{e}} = 1440$°C and

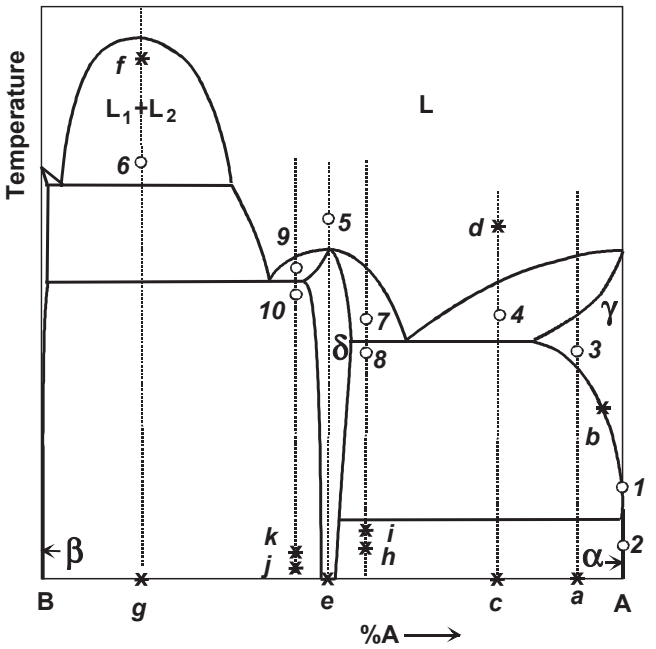

Fig. 9 The schematic binary phase diagram showing the points of HPT deformation or other thermal treatments (stars) and respective configuration points at the (increased) effective temperatures. The dashed vertical lines denote compositions of various alloys. Figurative points corresponding to the effective temperature of the alloys are indicated by an open circle and numbered. Each star point with a letter indicates the composition and temperature of an alloy's treatment (normal cooling, SPD or rapid quenching).

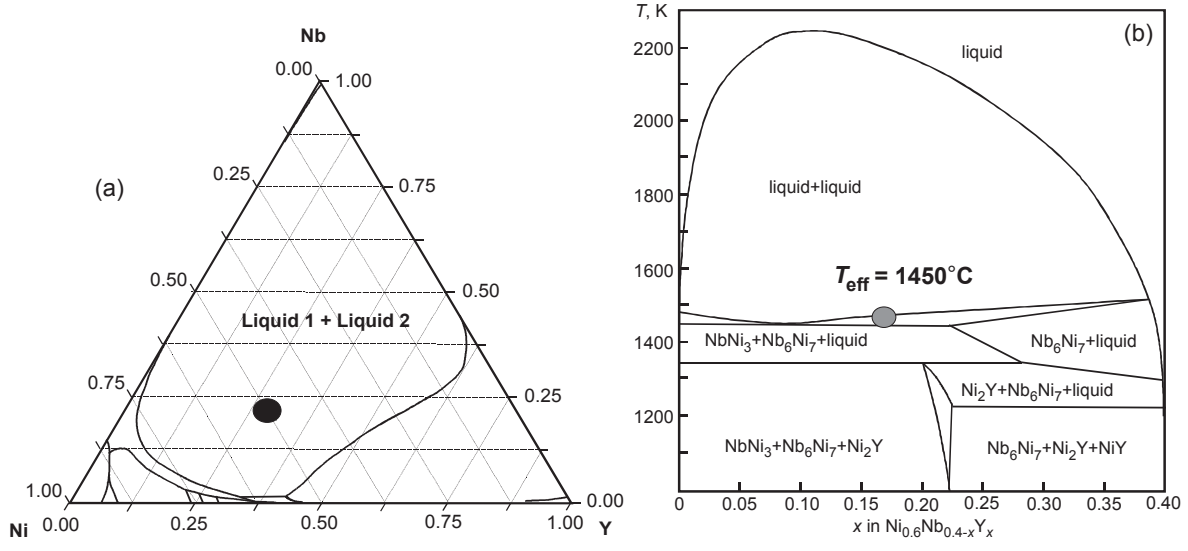

Fig. 10 (a) Liquidus projection obtained by the CALPHAD method of the Y–Ni–Nb ternary phase diagram at Ref. 95). The composition of the triple $Ni_{50}Nb_{20}Y_{30}$ alloy used for HPT investigations is marked by the large black circle. (b) Calculated pseudo-binary section of the ternary phase diagram $Ni_{60}Y_{40}$–$Ni_{60}Nb_{40}$.[96] Large grey circle shows the composition of phases in ultra-fine-grained alloy after HPT (two amorphous phases and two crystalline ones). The value of $T_{\text{eff}} = 400$°C is also given.

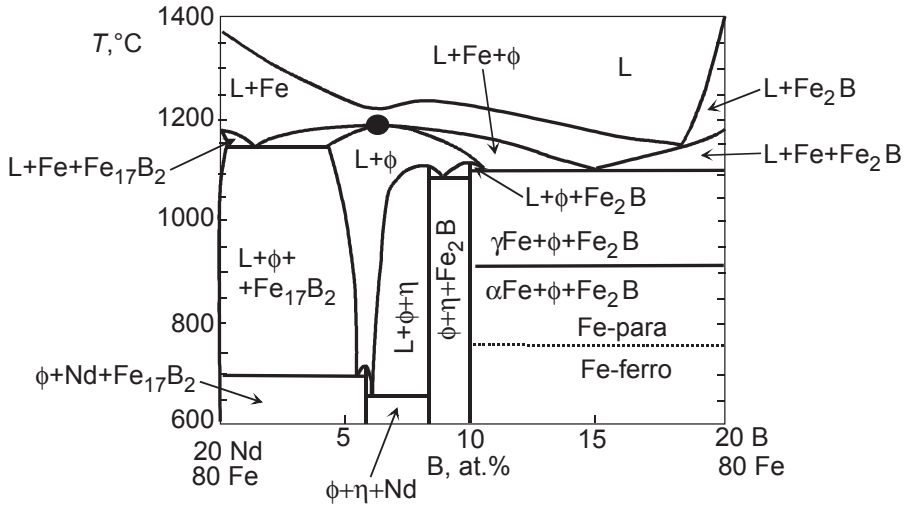

Fig. 11 The 80 at.% Fe section of the Fe–Nd–B phase diagram. Large filled circle shows the effective temperature $T_{eff} = 1170 \pm 30$°C.[7,8)]

can be estimated as $T_{eff} = 1450$°C (Fig. 10(a)). It is remarkable that the rapid solidification of these alloys from the liquid state (point *f*, Fig. 9) also allows obtaining the mixture of two amorphous phases.

In Refs. 7, 8) the HPT has been used for the treatment of liquid-phase sintered hard magnetic NdFeB-based alloy (5 GPa, 1 rpm, 5 rot, ambient temperature). The amorphization of the crystalline alloy took place under the action of HPT. This permitted to obtain for the first time the mixture of two different amorphous phases with embedded grains of the ferromagnetic $Nd_2Fe_{14}B$ phase. The SPD-treatment at ambient temperature $T_{SPD} = 300$ K is frequently equivalent to the heat treatment at a certain elevated temperature $T_{eff} > 300$ K. The composition of phases in the studied NdFeB-based alloy after HPT corresponds to the state at $T_{eff} \sim 1170$°C (Fig. 11).

Especially valuable data on the effective temperature at SPD can be extracted from the results on HPT treatment of Ti–48.5 at.% Ni, Ti–50.0 at.% Ni and Ti–50.7 at.% Ni alloys.[97)] The HPT of equiatomic Ti–50.0 at.% Ni alloy at room temperature (point *e*, Fig. 9) resulted in the fully amorphous state (point 5, Fig. 9, $T_{eff} = 1350$°C, respectively). The HPT of the non-equiatomic Ti–48.5 at.% Ni alloy at 270°C (point *h*) produced the mixture of amorphous and nanocrystalline phases (point 7, $T_{eff} = 1050$°C). When the HPT temperature of the Ti–48.5 at.% Ni alloy increased up to 350°C (point *h*), only the mixture of nanocrystaline phases formed, without amorphous phase. It means that the corresponding point moved from the position 7 in the δ+L region into position 8 in the two-phase $\delta+\gamma$ region and the effective temperature decreased to $T_{eff} = 950$°C. The HPT of another non-equiatomic Ti–50.7 at.% Ni alloy at 200°C (point *j*) produced the mixture of amorphous and nanocrystalline phases (point 9, $T_{eff} = 1250$°C). When the HPT temperature of the Ti–50.7 at.% Ni alloy increased up to 250°C (point *k*), only the mixture of nanocrystaline phases formed, without amorphous phase. It means that the corresponding point moved from the position 9 in the δ+L region into position 10 in the two-phase $\delta+\beta$ region and the effective temperature decreased to $T_{eff} = 1100$°C. Therefore, it can be clearly seen from the data obtained by Prokoshkin *et al.*[97)] that the increase of the HPT treatment temperature leads to the decrease of T_{eff}. It is in full accordance with the eq. (1) because the increase of T leads to increase of D_b, and at the same time the amount of deformation-driven atomic movements characterized by D_{HPT} remains unchanged. Other examples of amorhization under the action of SPD can be found in Refs. 98–103). Nanocrystallization is a process which is opposite to the amorphization. If one applies SPD to the initially amorphous sample, one can observe that the small nanocrystals start to appear.[104–112)] Obviously, the nanocrystallization and amorphization are also coupled and competing processes like precipitation/dissolution (see Section 3 above).

5. SPD-Driven Accelerated Mass-Transfer

The discussed SPD-driven phase transformations are connected with redistribution of components and, therefore, with mass transfer. This SPD-driven mass transfer is diffusion-like, in other words by the SPD-driven jump of an atom from one lattice position to another this atom has to overcome the same energetic barrier as during the conventional diffusion.

In Refs. 80, 87) we developed a mass-transfer model for the description of dynamic equilibrium in competitive precipitation and dissolution by the HPT in copper-silver system. This model assumes that HPT fixes the composition at interfaces between copper matrix and silver precipitate. It has been shown that the observed steady-state composition in the matrix and precipitate size are controlled by the HPT-enhanced diffusion-like mass-transfer. We succeeded to calculate the steady-state concentration c_{ss} using only the value of bulk diffusion coefficient D. Afterwards we found the T_{eff} value supposing that c_{ss} is equal to the silver solubility in copper at T_{eff}. As in the cases discussed above in Sections 3 and 4, T_{eff} in Cu–Ag alloys was higher than the HPT temperature T_{HPT}. The fact that usually $T_{eff} > T_{HPT}$ means simply that the steady-state concentration of vacancies during HPT is higher than the equilibrium one at T_{HPT}. It could be close to the equilibrium vacancy concentration at T_{eff}.[113,114)]

If one substitutes cobalt or silver in the copper-based solid solution, the bulk diffusion coefficient D of an impurity also changes. According to the eq. (1), the higher D would lead to the lower T_{eff} and lower D requires higher T_{eff}. Figure 8(a) contains the plot showing nearly linear correlation between activation enthalpy of bulk diffusion H_{D} and T_{eff}. Physically, such correlation is easy to understand because the high H_{D} means also high energy barrier for the jumps of alloying atoms between lattice positions in copper. Increased energy barrier for atomic jumps decreases the diffusivity and relaxation rate in the dynamic equilibrium between precipitation and dissolution during HPT. In turn, slow relaxation, increases the steady-state concentration of non-equilibrium lattice defects (vacancies). As a result, T_{eff} would increase as well.

The SPD-driven mass transfer proceeds extremely quickly and in ambient conditions without substantial increase of sample temperature.[115,116] Usually, the time for establishment of steady-state by HPT is about 2–5 minutes. It varies by change of pressure, strain rate and HPT temperature, but not more than one order of magnitude. One can estimate the observed SPD-driven mass-transfer using the effective diffusion coefficient and compare it with "conventional" diffusion coefficient at temperature of HPT-treatment and at T_{eff}.

The SPD-driven phase transformations can also be analyzed when assuming[1] that the *steady-state* concentration of lattice defects during SPD is higher than that in the equilibrium at the temperature of SPD-treatment, T_{SPD}, and pressure of the SPD-treatment, P_{SPD}. It has been indeed observed in the direct measurements of vacancy concentration during HPT.[115,117] This concentration would be equal to the *equilibrium* concentration of lattice defects at a certain effective temperature T_{eff}.[1] In case of Cu–Co system T_{eff} amounts to $T_{\text{eff}} = 900°\text{C}$ (Fig. 7). Figure 7 shows the composition of Cu-rich matrix in both alloys before and after HPT in the Cu–Co phase diagram. The Cu-rich solid solution in both alloys after HPT contains as much Co $c_{\text{eq}} \approx 2.5\,\text{wt.\%}$ Co, as if they would be annealed at $T_{\text{eff}} = 900°\text{C}$.

The extrapolation of bulk diffusion coefficients to T_{eff} gives $D = 5 \times 10^{-14}\,\text{m}^2/\text{s}$ for diffusion of Co in Cu[118] and $D = 10^{-13}\,\text{m}^2/\text{s}$ for self-diffusion in Cu.[119] Indeed, the deformation driven mechanisms can ensure the mass-transfer rate which is comparable to the bulk diffusion fluxes at $T_{\text{eff}} = 900°\text{C}$. The bulk diffusion fluxes at 900°C could ensure the decomposition/precipitation rates even if the effect of pressure is taken into account.[120,121]

6. Allotropic and Martensitic Transformations

Many elements exist in different allotropic modifications at different temperature and pressure. The most prominent examples are iron, cobalt, titanium. For example, the Co–Cu alloys before HPT contain the (metastable at room temperature) fcc α-Co phase, but after HPT the ε-Co phase appears in the samples.[1,59,60,122] Even more interesting is the situation in Ti, Zr and Hf where the high-pressure ω-phase exists.[123] The Ti, Zr and Hf possess also two different allotropic modifications at ambient pressure, namely the low-temperature hcp α-phase and high-temperature β-phase. HPT leads to the transitions of α- and β-phases to the ω-phase which remain in the samples after pressure release.[123–126] The alloying of titanium with β-stabilizers (like Fe, Co or Nb) strongly modifies the α-β-ω-transformations.[126–130] For example, the β-to-ω-transformation in Ti-alloys is martensitic.[126–128] There are special orientation relationships between β and ω lattices which ensure the diffusionless martensitic transformations where long-range mass transfer is not needed and the atoms conserve more or less their neighbors before and after transition.[131] It has been observed, for example, that iron addition changes the lattice parameters in β and ω phases in such a way that in the Ti–4 wt.% Fe alloy the orientation relationship fulfils optimally. At this concentration the amount of ω phases transformed from the β one reaches almost 100% and decreases by lower and higher Fe concentration.[126,127] The metastable ω-phase disappears by heating around 150°C in pure titanium. However, the alloying can stabilize it up to 500°C.[131,132]

HPT of silicon and germanium also leads to the formation of metastable high pressure phases.[133,134] In Ref. 135) the single crystalline Si(100) was subjected to HPT at 24 GPa at room temperature. The HPT-processed samples contained lattice defects such as dislocations and nanotwins in diamond-cubic Si-I, and metastable phases such as body-centered-cubic Si-III and hexagonal-diamond Si-IV. In Ref. 134) crystalline Ge disks were subjected to HPT under the nominal pressure of 24 GPa. The samples processed at room temperature consisted of diamond-cubic Ge-I and simple tetragonal Ge-III nanograins in addition to amorphous regions. The samples processed at 77 K consisted of Ge-I as well as residual Ge-III nanograins and some amorphous phase. No other metastable phases such as body-centered-cubic Ge-IV or hexagonal-diamond Ge-V were observed in the cryogenic HPT-processed sample.

Similar to the semiconductors Si and Ge, plastic deformation of oxides is generally very difficult due to their hard and brittle nature resulting from their covalent or ionic bonding. However, the HPT technique allows one to keep the silicon, germanium or oxide samples in the confined space, the samples cannot break of "escape" from the volume between the HPT anvils. This unique feature allows one to reach the high strains in the oxides. Moreover, one can start from powder samples. HPT first compacts the powder and then ensures the deformation. Thus, the opportunity to strain oxides and/or metal/oxide composites is very general.[136] However, here we discuss only the cases where oxides possess different crystal lattices and respective phase transitions can take place.

Crystalline VO_2 transformed from the coarse-grained monoclinic phase to a nanograined triclinic phase with insulating electrical properties by plastic strain effect.[137] The anatase-to-rutile phase transformation in TiO_2 usually occurs at 1173 K. During HPT of titania ceramic nanopowder the anatase-to-rutile transformation took place at 473–573 K.[138] The formation of rutile phase was accompanied with dynamic recrystallization and an unusual grain growth. A high-pressure TiO_2-II phase (columbite) with the orthorhombic structure was formed by HPT under pressures of 1 and 6 GPa. Fraction of TiO_2-II increased with increasing the plastic strain

and remained stable at ambient pressure. TiO_2-II was stabilized in grains with sizes less than ~15 nm because of high energy barrier for reverse phase transformation, while larger grains had the anatase structure.[139)]

Barium titanate, $BaTiO_3$ belongs to the group of perovskite oxides with the general ABO_3 formula. $BaTiO_3$ transforms under ambient pressure from a rhombohedral structure to an orthorhombic phase at −90°C, to a ferroelectric tetragonal phase at 5°C, and to a paraelectric cubic phase at 120°C.[140–143)] At ambient temperature, it exhibits a tetragonal-to-cubic phase transformation at 2 GPa[140–143)] and it disorders at 5 GPa.[144)] HPT of tetragonal $BaTiO_3$ powders leads to the formation of cubic phase and to strong grain refinement.[145)]

ZrO_2 has a monoclinic phase at room temperature under ambient pressure, and transforms to a tetragonal phase at 1373 K, a cubic phase at 2673 K, a liquid phase at 2963 K and an orthorhombic phase under pressures above 10 GPa.[146)] However, addition of specific elements such as Y to ZrO_2 stabilizes the tetragonal phase at room temperature.[147)] This partially stabilized ZrO_2 exhibits a phase transformation from tetragonal to monoclinic.[148)] During HPT the transformation with a coherent interface occurs from the metastable tetragonal phase to the monoclinic phase.[149)]

7. Grain Boundary Phase Transitions

Severe plastic deformation drives not only phase transformations between 3-dimensional or bulk phases discussed above. SPD can also lead to the various grain boundary (GB) phase transitions. The most prominent GB phase transformations like wetting-dewetting ones take place in the two-phase (or multiphase) regions of the bulk phase diagrams.[150)] In case of complete wetting, the second phase (liquid or even solid one) forms the continous layer between two grains in the matrix.[13,24,151)] In this case the contact angle between GB and second phase is zero.[152)] In case of incomplete (or partial) wetting, the second phase (liquid or solid) forms the chain of individual particles along GB with a certain non-zero contact angle.[153,154)] If the amount of wetting phase is small, the continous layer between two grains can become very thin, it contains few monolayers of a second component and is just a couple of nanometers thick.[155–157)] If the amount of a second component in GB is below one monolayer, one speaks about conventional GB adsorption.[157,158)] If the GB contact angle is high, but the GB between individual particles of a second phase contains few monolayers of a second component, one speaks about pseudopartial (or psedoincomplete, or constrained complete) GB wetting.[159–161)] The transitions between these different GB states (phases) are called GB transitions, and they also can be driven by SPD, similar to the bulk (or volume) ones.

The grain size after SPD is very small. In other words, the specific area of grain boundaries in a volume unit increases. Therefore, the "conventional" grain boundary phase transitions become more pronounced then in the coarse-grained materials. For example, the usage of the ultrafine-grained polycrystals made it possible to observe and measure the thermal effect of the GB premelting phase transformations.[162–165)] In other words, the liquid-like GB layers form well below the bulk solidus line. As a result, the melting in GBs begins during heating 10–15°C earlier than in the bulk.[162–165)] Between bulk and GB solidus the (generally solid) polycrystal contains thin liquid GBs. Such a materials possesses extremely high plasticity.[166–171)] The high specific density of GBs in the SPD-treated alloys allowed one also to observe the thermal effect of phase transition from incomplete to complete GB wetting.[163–165)] It takes place between bull solidus and liquidus lines.

Even in case of one-layer GB adsorption (i.e. when the concentration of a second component per GB unit area is below one monolayer), the specific area of GBs in SPD-treated polycrystals is so high that a big amount of a second component is needed to fill all GB adsorption layers. These adsorbed GB atoms are taken away from the bulk second phase. As a result, the amount of bulk second phase decreases, it can disappear completely (like, for example, disappears cementite in steels). In such a way, the GB adsorption can apparently shift the lines in the bulk phase diagrams for the ultra-fine grained materials in comparison with their coarse-grained counterparts.[170–174)]

The HPT of the Al–Zn, Al–Mg and Al–Zn–Mg alloys leads to the formation of 2–5 nm thin GB layers of Zn-rich phase.[75,175–183)] The contact angle between Zn particles and GB is high, the GB between individual particles of a second phase contains few monolayers of a second component. In other words, here one can speaks about pseudopartial GB wetting.[159–161)] The presence of "soft" Zn-rich GB layers between grains of "hard" phase leads to a kind of lubricating during GB sliding. As a result, the ultrafine-grained Al-based alloys become superductile.[176–178,180–183)] The opposite effect can also take place. Thus, the second solid phase can form before HPT the continous layers in GBs of a matrix (so-called complete GB wetting). If this phase is hard (like for example in case of Cu–Sn or Mg-based alloys), the soft matrix deform during HPT and its grains are refined, but the hard skeleton of intermetallics in the initial GBs remain more or less intact and ensure the high hardness of an alloy.[13,24,76,79)] All these SPD-driven GB phenomena are now under intensive investigations.

8. Conclusions

It is frequently observed that the phases in the materials after severe plastic deformation differ from those in the initial state. During SPD established a steady-state, and structure and properties of a material in this steady state do not depend on the initial state and are, therefore, equifinal. The SPD-induced phase transformations proceed very quickly, they include precipitation and dissolution of precipitates, amorphization and (nano) crystallization, allotropic and martensitic transitions and formation of grain boundary phases.

Acknowledgements

The authors are deeply grateful to Profs. H. Hahn, P. Zięba, Drs. Yu. Ivanisenko, A. Gornakova and A. Korneva for valuable suggestions and discussion. The work is partially supported by the Russian Science Foundation under grant 17-72-10304 (P. Straumal, discussion of Mg alloys) and

performed in National University of Science and Technology MISiS. It was also partially supported by the state task of ISSP and CSC RAS (A. Mazilkin, B. Straumal, A. Kilmametov, discussion of Cu, Al and Ti alloys).

REFERENCES

1) B.B. Straumal, A.A. Mazilkin, B. Baretzky, E. Rabkin and R.Z. Valiev: Mater. Trans. **53** (2012) 63–71.
2) X. Sauvage, A. Chbihi and X. Quelennec: J. Phys.: Conf. Ser. **240** (2010) 012003.
3) B. Straumal, A. Korneva and P. Zięba: Arch. Civ. Mech. Eng. **14** (2014) 242–249.
4) E.I. Teitel', L.S. Metlov, D.V. Gunderov and A.V. Korznikov: Phys. Met. Metallogr. **113** (2012) 1162–1168.
5) B.B. Straumal, A.R. Kilmametov, Yu. Ivanisenko, A.A. Mazilkin, O.A. Kogtenkova, L. Kurmanaeva, A. Korneva, P. Zięba and B. Baretzky: Int. J. Mater. Res. **106** (2015) 657–664.
6) B.B. Straumal, A.R. Kilmametov, A. Korneva, A.A. Mazilkin, P.B. Straumal, P. Zięba and B. Baretzky: J. Alloys Compd. **707** (2017) 20–26.
7) B.B. Straumal, A.R. Kilmametov, A.A. Mazilkin, S.G. Protasova, K.I. Kolesnikova, P.B. Straumal and B. Baretzky: Mater. Lett. **145** (2015) 63–66.
8) B.B. Straumal, A.A. Mazilkin, S.G. Protasova, D.V. Gunderov, G.A. López and B. Baretzky: Mater. Lett. **161** (2015) 735–739.
9) C. Borchers, C. Garve, M. Tiegel, M. Deutges, A. Herz, K. Edalati, R. Pippan, Z. Horita and R. Kirchheim: Acta Mater. **97** (2015) 207–215.
10) S. Lee and Z. Horita: Mater. Trans. **53** (2012) 38–45.
11) K. Edalati, S. Toh, M. Watanabe and Z. Horita: Scr. Mater. **66** (2012) 386–389.
12) J.M. Cubero-Sesin and Z. Horita: Mater. Trans. **53** (2012) 46–55.
13) K. Bryła, J. Morgiel, M. Faryna, K. Edalati and Z. Horita: Mater. Lett. **212** (2018) 323–326.
14) A.A. Mazilkin, B.B. Straumal, S.G. Protasova, O.A. Kogtenkova and R.Z. Valiev: Phys. Solid State **49** (2007) 868–873.
15) B.B. Straumal, O.A. Kogtenkova, S.G. Protasova, P. Zięba, T. Czeppe, B. Baretzky and R.Z. Valiev: J. Mater. Sci. **46** (2011) 4243–4247.
16) K. Edalati, D.J. Lee, T. Nagaoka, M. Arita, H.S. Kim, Z. Horita and R. Pippan: Mater. Trans. **57** (2016) 533–538.
17) K. Edalati, Y. Hashiguchi, P.H.R. Pereirac, Z. Horita and T.G. Langdon: Mater. Sci. Eng. A **714** (2018) 167–171.
18) K. Edalati and Z. Horita: Acta Mater. **59** (2011) 6831–6836.
19) K. Edalati, Z. Horita, T. Furuta and S. Kuramoto: Mater. Sci. Eng. A **559** (2013) 506–509.
20) A.A. Mazilkin, O.A. Kogtenkova, B.B. Straumal, R.Z. Valiev and B. Baretzky: Def. Diff. Forum **237–240** (2005) 739–744.
21) A.A. Mazilkin, B. Baretzky, S. Enders, O.A. Kogtenkova, B.B. Straumal, E.I. Rabkin and R.Z. Valiev: Def. Diff. Forum **249** (2006) 155–160.
22) R. Kulagin, Y. Beygelzimer, Yu. Ivanisenko, A. Mazilkin, B. Straumal and H. Hahn: Mater. Lett. **222** (2018) 172–175.
23) R.Z. Valiev, R.K. Islamgaliev and I.V. Alexandrov: Prog. Mater. Sci. **45** (2000) 103–189.
24) K. Bryła, M. Krystian, J. Horky, B. Mingler, K. Mroczka, P. Kurtyka and L. Lityńska-Dobrzyńska: Mater. Sci. Eng. A **737** (2018) 318–327.
25) E.A. Lukyanova, N.S. Martynenko, V.N. Serebryany, A.N. Belyakov, L.L. Rokhlin, S.V. Dobatkin and Y.Z. Estrin: Russ. Metall. **2017** (2017) 912–921.
26) P. Kral, J. Dvorak, V. Sklenicka, T. Masuda, Z. Horita, K. Kucharova, M. Kvapilova and M. Svobodova: Mater. Sci. Eng. A **723** (2018) 287–295.
27) S. Sabbaghianrad, S.A. Torbati-Sarraf and T.G. Langdon: Mater. Sci. Eng. A **712** (2018) 373–379.
28) K. Tirsatine, H. Azzeddine, Y. Huang, T. Baudin, A.-L. Helbert, F. Brisset, D. Bradai and T.G. Langdon: J. Alloys Compd. **753** (2018) 46–53.
29) M.Y. Alawadhi, S. Sabbaghianrad, Y. Huanga and T.G. Langdon: J. Mater. Rest. Technol. **6** (2017) 369–377.
30) M. Azabou, T. Makhlouf, J. Saurin, L. Escoda, J.J. Suñol and M. Khitouni: Int. J. Adv. Manuf. Technol. **87** (2016) 981–987.
31) A.A. Mazilkin, B.B. Straumal, E. Rabkin, B. Baretzky, S. Enders, S.G. Protasova, O.A. Kogtenkova and R.Z. Valiev: Acta Mater. **54** (2006) 3933–3939.
32) B. Straumal, A.R. Kilmametov, Yu.O. Kucheev, L. Kurmanaeva, Yu. Ivanisenko, B. Baretzky, A. Korneva, P. Zięba and D.A. Molodov: Mater. Lett. **118** (2014) 111–114.
33) Y. Huang, S. Sabbaghianrad, A.I. Almazrouee, K.J. Al-Fadhalah, S.N. Alhajeri and T.G. Langdon: Mater. Sci. Eng. A **656** (2016) 55–66.
34) N. Lugo, N. Llorca, J.M. Cabrera and Z. Horita: Mater. Sci. Eng. A **477** (2008) 366–371.
35) J. Čížek, M. Janeček, O. Srba, R. Kužel, Z. Barnovská, I. Procházka and S. Dobatkin: Acta Mater. **59** (2011) 2322–2329.
36) X.Z. Liao, Y.H. Zhao, Y.T. Zhu, R.Z. Valiev and D.V. Gunderov: J. Appl. Phys. **96** (2004) 636–640.
37) M. Shamsborhan and M. Ebrahimi: J. Alloys Compd. **682** (2016) 552–556.
38) C.L. Tang, H. Li and S.Y. Li: Trans. Nonferr. Met. Soc. China **26** (2016) 1736–1744.
39) Z.N. Mao, R.C. Gu, F. Liu, Y. Liu, X.Z. Liao and J.T. Wang: Mater. Sci. Eng. A **674** (2016) 186–192.
40) E. Bagherpour, F. Qods, R. Ebrahimi and H. Miyamoto: Mater. Sci. Eng. A **674** (2016) 221–231.
41) E. Bagherpour, F. Qods, R. Ebrahimi and H. Miyamoto: Mater. Sci. Eng. A **666** (2016) 324–338.
42) P.C. Yadav, A. Sinhal, S. Sahu, A. Roy and S. Shekhar: J. Mater. Eng. Perform. **25** (2016) 2604–2614.
43) C. Xu, Z. Horita and T.G. Langdon: Mater. Sci. Eng. A **528** (2011) 6059–6065.
44) K. Edalati and Z. Horita: Mater. Sci. Eng. A **528** (2011) 7514–7523.
45) A.V. Korznikov, Y.V. Ivanisenko, D.V. Laptionok, I.M. Safarov, V.P. Pilyugin and R.Z. Valiev: Nanostruct. Mater. **4** (1994) 159–167.
46) Y. Ivanisenko, W. Lojkowski, R.Z. Valiev and H.-J. Fecht: Acta Mater. **51** (2003) 5555–5570.
47) Y. Ivanisenko, R.K. Wunderlich, R.Z. Valiev and H.-J. Fecht: Scr. Mater. **49** (2003) 947–952.
48) J. Zrnik, R. Pippan, S. Scheriau, L. Kraus and M. Fujda: J. Mater. Sci. **45** (2010) 4822–4826.
49) S. Bayramoglu, C.H. Gür, I.V. Alexandrov and M.M. Abramova: Mater. Sci. Eng. A **527** (2010) 927–933.
50) J. Ning, E. Courtois-Manara, L. Kurmanaeva, A.V. Ganeev, R.Z. Valiev, C. Kübel and Y. Ivanisenko: Mater. Sci. Eng. A **581** (2013) 8–15.
51) Y. Todaka, Y. Miki, M. Umemoto, C. Wang and K. Tsuchiya: Mater. Sci. Forum **584–586** (2008) 597–602.
52) X.Z. Liao, A.R. Kilmametov, R.Z. Valiev, H. Gao, X. Li, A.K. Mukherjee, J.F. Bingert and Y.T. Zhu: Appl. Phys. Lett. **88** (2006) 021909.
53) R. Pippan, S. Scheriau, A. Taylor, M. Hafok, A. Hohenwarter and A. Bachmaier: Annu. Rev. Mater. Res. **40** (2010) 319–343.
54) H. Wen, R.K. Islamgaliev, K.M. Nesterov, R.Z. Valiev and E.J. Lavernia: Philos. Mag. Lett. **93** (2013) 481–489.
55) K. Edalati, D. Akama, A. Nishio, S. Lee, Y. Yonenaga, J.M. Cubero-Sesin and Z. Horita: Acta Mater. **69** (2014) 68–77.
56) R. Tejedor, K. Edalati, J.A. Benito, Z. Horita and J.M. Cabrera: Mater. Sci. Eng. A **743** (2019) 597–605.
57) I.F. Mohamed, T. Masuda, S. Lee, K. Edalati, Z. Horita, S. Hirosawa, K. Matsuda, D. Terada and M.Z. Omar: Mater. Sci. Eng. A **704** (2017) 112–118.
58) K. Edalati, H. Shao, H. Emami, H. Iwaoka, E. Akiba and Z. Horita: Int. J. Hydr. Ener. **41** (2016) 8917–8924.
59) M. Isik, M. Niinomi, K. Cho, M. Nakai, H. Liu, H. Yilmazer, Z. Horita, S. Sato and T. Narushima: J. Mech. Behav. Biomed. Mater. **59** (2016) 226–235.
60) M. Isik, M. Niinomi, H. Liu, K. Cho, M. Nakai, Z. Horita, S. Sato, T. Narushima, H. Yilmazer and M. Nagasako: Mater. Trans. **57** (2016) 1109–1118.
61) T. Hongo, K. Edalati, H. Iwaoka, M. Arita, J. Matsuda, E. Akiba and Z. Horita: Mater. Sci. Eng. A **618** (2014) 1–8.
62) K. Edalati, K. Imamura, T. Kiss and Z. Horita: Mater. Trans. **53** (2012)

123–127.
63) A. Hanna, H. Azzeddine, R. Lachha, T. Baudin, A.-L. Helbert, F. Brisset, Y. Huang, D. Bradai and T.G. Langdon: J. Alloys Compd. **778** (2019) 61–71.
64) Y.I. Bourezg, H. Azzeddine, T. Baudin, A.-L. Helbert, Y. Huang, D. Bradai and T.G. Langdon: Mater. Sci. Eng. A **724** (2018) 477–485.
65) P. Bazarnik, Y. Huang, M. Lewandowska and T.G. Langdon: Mater. Sci. Eng. A **712** (2018) 513–520.
66) D.M.M. Cardona, J. Wongsa-Ngam, H. Jimenez and T.G. Langdon: J. Mater. Rest. Technol. **6** (2017) 355–360.
67) S.A. Torbati-Sarraf, S. Sabbaghianrad, R.B. Figueiredo and T.G. Langdon: J. Alloys Compd. **712** (2017) 185–193.
68) M. Diez, H.-E. Kim, V. Serebryany, S. Dobatkin and Y. Estrin: Mater. Sci. Eng. A **612** (2014) 287–292.
69) E.A. Lukyanova, N.S. Martynenko, I. Shakhova, A.N. Belyakov, L.L. Rokhlin, S.V. Dobatkin and Y.Z. Estrin: Mater. Lett. **170** (2016) 5–9.
70) N.S. Martynenko, E.A. Luk'yanova, M.M. Morozov, V.S. Yusupov, S.V. Dobatkin and Y.Z. Estrin: Met. Sci. Heat Treat. **60** (2018) 253–258.
71) C.C. Koch, T.G. Langdon and E.J. Lavernia: Metall. Mater. Trans. A **48** (2017) 5181–5199.
72) A.A. Mazilkin, B.B. Straumal, M.V. Borodachenkova, R.Z. Valiev, O.A. Kogtenkova and B. Baretzky: Mater. Lett. **84** (2012) 63–65.
73) B.B. Straumal, B. Baretzky, A.A. Mazilkin, F. Phillipp, O.A. Kogtenkova, M.N. Volkov and R.Z. Valiev: Acta Mater. **52** (2004) 4469–4478.
74) Y. Ito, K. Edalati and Z. Horita: Mater. Sci. Eng. A **679** (2017) 428–434.
75) X. Sauvage, M.Yu. Murashkin, B.B. Straumal, E. Bobruk and R.Z. Valiev: Adv. Eng. Mater. **17** (2015) 1821–1827.
76) V.D. Sitdikov, P.S. Chizhov, M.Yu. Murashkin and R.Z. Valiev: Rev. Adv. Mater. Sci. **47** (2016) 59–65.
77) A. Korneva, O. Kogtenkova, S. Protasova, B. Straumal, A. Mazilkin, L. Kurmanaeva and P. Zięba: Inżyn. Materiał. **34** (4–126) (2013) 306–309.
78) B.B. Straumal, S.G. Protasova, A.A. Mazilkin, O.A. Kogtenkova, L. Kurmanaeva, B. Baretzky, G. Schütz, A. Korneva and P. Zięba: Mater. Lett. **98** (2013) 217–221.
79) L. von Bertalanffy: Science **111** (1950) 23–29.
80) B.B. Straumal, S.G. Protasova, A.A. Mazilkin, E. Rabkin, D. Goll, G. Schütz, B. Baretzky and R. Valiev: J. Mater. Sci. **47** (2012) 360–367.
81) B.B. Straumal, A.R. Kilmametov, Yu.O. Kucheev, K.I. Kolesnikova, A. Korneva, P. Zięba and B. Baretzky: JETP Lett. **100** (2014) 376–379.
82) A. Korneva, B. Straumal, R. Chulist, A. Kilmametov, P. Bała, G. Cios, N. Schell and P. Zięba: Mater. Lett. **179** (2016) 12–15.
83) A. Korneva, B. Straumal, A. Kilmametov, G. Cios, P. Bała and P. Zięba: Mater. Charact. **118** (2016) 411–416.
84) A. Korneva, B. Straumal, O. Kogtenkova, Yu. Ivanisenko, A. Wierzbicka-Miernik, A. Kilmametov and P. Zięba: IOP Conf. Ser.: Mater. Sci. Eng. **63** (2014) 012093.
85) B.B. Straumal, A.R. Kilmametov, A.A. Mazilkin, L. Kurmanaeva, Y. Ivanisenko, A. Korneva, P. Zięba and B. Baretzky: Mater. Lett. **138** (2015) 255–258.
86) A. Korneva, B. Straumal, A. Kilmametov, R. Chulist, P. Straumal and P. Zięba: Mater. Charact. **114** (2016) 151–156.
87) B.B. Straumal, V. Pontikis, A.R. Kilmametov, A.A. Mazilkin, S.V. Dobatkin and B. Baretzky: Acta Mater. **122** (2017) 60–71.
88) A. Korneva, B. Straumal, A. Kilmametov, R. Chulist, G. Cios, B. Baretzky and P. Zięba: Materials **12** (2019) 447.
89) B.B. Straumal, A.R. Kilmametov, O.A. Kogtenkova, A.A. Mazilkin, B. Baretzky, A. Korneva and P. Zięba: Int. J. Mater. Res. **110** (2019), in press.
90) G.A. López, I. López-Ferreño, A.R. Kilmametov, T. Breczewski, B.B. Straumal, B. Baretzky, M.L. Nó and J. San Juan: Mater. Today: Procs. **2S** (2015) S747–S750.
91) B.B. Straumal, A.R. Kilmametov, G.A. López, I. López-Ferreño, M.L. Nó, J. San Juan, H. Hahn and B. Baretzky: Acta Mater. **125** (2017) 274–285.
92) G. Martin: Phys. Rev. B **30** (1984) 1424–1436.
93) B.B. Straumal, A.A. Mazilkin, S.G. Protasova, D. Goll, B. Baretzky, A.S. Bakai and S.V. Dobatkin: Kovove Materialy-Metallic Materials **49** (2011) 17–22.
94) A.A. Mazilkin, G.E. Abrosimova, S.G. Protasova, B.B. Straumal, G. Schütz, S.V. Dobatkin and A.S. Bakai: J. Mater. Sci. **46** (2011) 4336–4342.
95) U.R. Kattner: JOM **49** (1997) 14–19.
96) N. Mattern, U. Kühn, A. Gebert, A. Schoeps, T. Gemminga and L. Schultz: Mater. Sci. Eng. A **449–451** (2007) 207–210.
97) S.D. Prokoshkin, I.Yu. Khmelevskaya, S.V. Dobatkin, I.B. Trubitsyna, E.V. Tatyanin, V.V. Stolyarov and E.A. Prokofiev: Acta Mater. **53** (2005) 2703–2714.
98) A.V. Sergueeva, C. Song, R.Z. Valiev and A.K. Mukherjee: Mater. Sci. Eng. A **339** (2003) 159–165.
99) X. Sauvage, L. Renaud, B. Deconihout, D. Blavette, D.H. Ping and K. Hono: Acta Mater. **49** (2001) 389–394.
100) T. Miyazaki, D. Terada, Y. Miyajima, C. Suryanarayana, R. Murao, Y. Yokoyama, K. Sugiyama, M. Umemoto, T. Todaka and N. Tsuji: J. Mater. Sci. **46** (2011) 4296–4301.
101) V.V. Stolyarov, D.V. Gunderov, A.G. Popov, V.S. Gaviko and A.S. Ermolenko: J. Alloys Compd. **281** (1998) 69–71.
102) Y. Matsuura, S. Hirosawa, H. Yamamoto, S. Fujimira, M. Sagawa and K. Osamura: Jpn. J. Appl. Phys. **24** (1985) L635–L637.
103) Á. Révész, S. Hóbor, J.L. Lábár, A.P. Zhilyaev and Zs. Kovácz: J. Appl. Phys. **100** (2006) 103522.
104) A.M. Glezer, M.R. Plotnikova, A.V. Shalimova and S.V. Dobatkin: Bull. Russ. Acad. Sci., Physics **73** (2009) 1233.
105) S. Hóbor, Á. Révész, A.P. Zhilyaev and Zs. Kovácz: Rev. Adv. Mater. Sci. **18** (2008) 590–592.
106) Zs. Kovács, P. Henits, A.P. Zhilyaev and Á. Révész: Scr. Mater. **54** (2006) 1733–1737.
107) G.E. Abrosimova, A.S. Aronin, S.V. Dobatkin, S.D. Kaloshkin, D.V. Matveev, O.G. Rybchenko, E.V. Tatyanin and I.I. Zverkova: J. Metastab. Nanocryst. Mater. **24** (2005) 69–72.
108) Á. Révész, E. Schafler and Zs. Kovács: Appl. Phys. Lett. **92** (2008) 011910.
109) S. Hóbor, Zs. Kovács, A.P. Zhilyaev, L.K. Varga, P.J. Szabó and Á. Révész: J. Phys.: Conf. Ser. **240** (2010) 012153.
110) S. Hóbor, Á. Révész, P.J. Szabó, A.P. Zhilyaev, V. Kovács Kis, J.L. Lábár and Zs. Kovács: J. Appl. Phys. **104** (2008) 033525.
111) P. Henits, Á. Révész, A.P. Zhilyaev and Zs. Kovács: J. Alloys Compd. **461** (2008) 195–199.
112) Zs. Kovács, P. Henits, A.P. Zhilyaev, N.Q. Chinh and Á. Révész: Mater. Sci. Forum **519–521** (2006) 1329–1334.
113) B. Oberdorfer, E.-M. Steyskal, W. Sprengel, W. Puff, M. Zehetbauer, R. Pippan and R. Wuerschum: Phys. Rev. Lett. **105** (2010) 146101.
114) J. Čížek, O. Melikhova, Z. Barnovská, I. Procházka and R.K. Islamgaliev: J. Phys. Conf. Ser. **443** (2013) 012008.
115) B.B. Straumal, O.A. Kogtenkova, R.Z. Valiev, P. Zięba and B. Baretzky: Diff. Found. **5** (2015) 95–108.
116) T. Ungár, E. Schafler, P. Hanak, S. Bernstorff and M. Zehetbauer: Mater. Sci. Eng. A **462** (2007) 398–401.
117) T. Ungár, E. Schafler, P. Hanák, S. Bernstorff and M. Zehetbauer: Z. Metallk. **96** (2005) 578–583.
118) C.A. Mackliet: Phys. Rev. **109** (1958) 1964–1970.
119) S. Fujikawa and K.I. Hirano: Proc. of Yamada Vth Conf. on Point Defects, Defect Interactions in Metals, ed. by J.I. Takamura, M. Doyama and M. Kiritani, (Univ. of Tokyo Press, 1982) pp. 554–558.
120) D.A. Molodov, B.B. Straumal and L.S. Shvindlerman: Scr. Metall. **18** (1984) 207–211.
121) B.B. Straumal, L.M. Klinger and L.S. Shvindlerman: Scr. Metall. **17** (1983) 275–279.
122) B.B. Straumal, S.G. Protasova, A.A. Mazilkin, B. Baretzky, D. Goll, D.V. Gunderov and R.Z. Valiev: Philos. Mag. Lett. **89** (2009) 649–654.
123) B.B. Straumal, A.S. Gornakova, A.A. Mazilkin, O.B. Fabrichnaya, M.J. Kriegel, B. Baretzky, J.-Z. Jiang and S.V. Dobatkin: Mater. Lett. **81** (2012) 225–228.
124) B.B. Straumal, A.S. Gornakova, O.B. Fabrichnaya, M.J. Kriegel, A.A. Mazilkin, B. Baretzky, A.M. Gusak and S.V. Dobatkin: High Temp. Mater. Proc. **31** (2012) 339–350.
125) A. Kilmametov, Yu. Ivanisenko, B.B. Straumal, A.A. Mazilkin, A.S.

Gornakova, M.J. Kriegel, O.B. Fabrichnaya, D. Rafaja and H. Hahn: Scr. Mater. **136** (2017) 46–49.
126) A. Kilmametov, Yu. Ivanisenko, A.A. Mazilkin, B.B. Straumal, A.S. Gornakova, O.B. Fabrichnaya, M.J. Kriegel, D. Rafaja and H. Hahn: Acta Mater. **144** (2018) 337–351.
127) B.B. Straumal, A.R. Kilmametov, Yu. Ivanisenko, A.A. Mazilkin, R.Z. Valiev, N.S. Afonikova, A.S. Gornakova and H. Hahn: J. Alloys Compd. **735** (2018) 2281–2286.
128) A.R. Kilmametov, Yu. Ivanisenko, B.B. Straumal, A.S. Gornakova, A.A. Mazilkin and H. Hahn: Metals **8** (2018) 1–12.
129) A.S. Gornakova, A.B. Straumal, I.I. Khodos, I.B. Gnesin, A.A. Mazilkin, N.S. Afonikova and B.B. Straumal: J. Appl. Phys. **125** (2019) 082522.
130) B.B. Straumal, A. Korneva, A.R. Kilmametov, L. Lityńska-Dobrzyńska, A.S. Gornakova, R. Chulist, M.I. Karpov and P. Zięba: Materials **12** (2019) 426.
131) B.B. Straumal, A.R. Kilmametov, Yu. Ivanisenko, A.S. Gornakova, A.A. Mazilkin, M.J. Kriegel, O.B. Fabrichnaya, B. Baretzky and H. Hahn: Adv. Eng. Mater. **17** (2015) 1835–1841.
132) M.J. Kriegel, A. Kilmametov, M. Rudolph, B.B. Straumal, A.S. Gornakova, H. Stöcker, Y. Ivanisenko, O. Fabrichnaya, H. Hahn and D. Rafaja: Adv. Eng. Mater. **20** (2018) 1700933.
133) B. Chon, Y. Ikoma, M. Kohno, J. Shiomi, M.R. McCartney, D.J. Smith and Z. Horita: Scr. Mater. **157** (2018) 120–123.
134) Y. Ikoma, K. Kumano, K. Edalati, M.R. McCartney, D.J. Smith and Z. Horita: Mater. Charact. **132** (2017) 132–138.
135) Y. Fukushima, Y. Ikoma, K. Edalati, B. Chon, D.J. Smith and Z. Horita: Mater. Charact. **129** (2017) 163–168.
136) Y. Qi, A. Kosinova, A.R. Kilmametov, B.B. Straumal and E. Rabkin: Mater. Charact. **145** (2018) 389–401.
137) K. Edalati, I. Fujita, X. Sauvage, M. Arita and Z. Horita: J. Alloys Compd. **779** (2019) 394–398.
138) K. Edalati, Q. Wang, H. Razavi-Khosroshahi, H. Emami, M. Fuji and Z. Horita: Scr. Mater. **162** (2019) 341–344.
139) H. Razavi-Khosroshahi, K. Edalati, M. Arita, Z. Horita and M. Fuji: Scr. Mater. **124** (2016) 59–62.
140) W. Zhong, D. Venderbilt and K.M. Rabe: Phys. Rev. Lett. **73** (1994) 1861–1864.
141) T. Ishidate, S. Abe, H. Takahashi and N. Mori: Phys. Rev. Lett. **78** (1997) 2397–2400.
142) S.A. Hayward and E.K.H. Salje: J. Phys.: Condens. Matter **14** (2002) L599–L604.
143) J.J. Wang, P.P. Wu, X.Q. Ma and L.Q. Chen: J. Appl. Phys. **108** (2010) 114105.
144) U.D. Venkateswaran, V.M. Naik and R. Naik: Phys. Rev. B **58** (1998) 14256–14260.
145) K. Edalati, M. Arimura, Y. Ikoma, T. Daio, M. Miyata, D.J. Smith and Z. Horita: Mater. Res. Lett. **3** (2015) 216–221.
146) R.C. Garvie, R.H.J. Hannink and R.T. Pascoe: Nature **258** (1975) 703–704.
147) R.H.J. Hannink, P.M. Kelly and B.C. Muddle: J. Am. Ceram. Soc. **83** (2000) 461–487.
148) J.M. Leger, P.E. Tomaszewski, A. Atouf and A.S. Pereira: Phys. Rev. B **47** (1993) 14075–14083.
149) K. Edalati, S. Toh, Y. Ikoma and Z. Horita: Scr. Mater. **65** (2011) 974–977.
150) E.I. Rabkin, L.S. Shvindlerman and B.B. Straumal: Int. J. Mod. Phys. B **5** (1991) 2989–3028.
151) B.B. Straumal, O.I. Noskovich, V.N. Semenov, L.S. Shvindlerman, W. Gust and B. Predel: Acta Metall. Mater. **40** (1992) 795–801.
152) B.B. Straumal, W. Gust and T. Watanabe: Mater. Sci. Forum **294–296** (1999) 411–414.
153) B.B. Straumal, A.A. Mazilkin, S.G. Protasova, A.M. Gusak, M.F. Bulatov, A.B. Straumal and B. Baretzky: Rev. Adv. Mater. Sci. **38** (2014) 17–28.
154) A.B. Straumal, K.V. Tsoi, I.A. Mazilkin, A.N. Nekrasov and K. Bryła: Arch. Metall. Mater. **64** (2019), in press.
155) L.-S. Chang, B.B. Straumal, E. Rabkin, W. Gust and F. Sommer: J. Phase Equil. **18** (1997) 128–135.
156) L.-S. Chang, E. Rabkin, B. Straumal, P. Lejcek, S. Hofmann and W. Gust: Scr. Mater. **37** (1997) 729–735.
157) L.-S. Chang, E. Rabkin, B.B. Straumal, S. Hoffmann, B. Baretzky and W. Gust: Defect Diff. Forum **156** (1998) 135–146.
158) B.B. Straumal, P. Zięba and W. Gust: Int. J. Inorg. Mater. **3** (2001) 1113–1115.
159) B.B. Straumal, A.O. Rodin, A.E. Shotanov, A.B. Straumal, O.A. Kogtenkova and B. Baretzky: Def. Diff. Forum **333** (2013) 175–192.
160) B.B. Straumal, A.A. Mazilkin, S.G. Protasova, G. Schütz, A.B. Straumal and B. Baretzky: J. Mater. Eng. Perform. **25** (2016) 3303–3309.
161) B.B. Straumal, A.A. Mazilkin and B. Baretzky: Curr. Opin. Solid State Mater. Sci. **20** (2016) 247–256.
162) B. Straumal, R. Valiev, O. Kogtenkova, P. Zieba, T. Czeppe, E. Bielanska and M. Faryna: Acta Mater. **56** (2008) 6123–6131.
163) O.A. Kogtenkova, S.G. Protasova, A.A. Mazilkin, B.B. Straumal, P. Zięba, T. Czeppe and B. Baretzky: J. Mater. Sci. **47** (2012) 8367–8371.
164) O.A. Kogtenkova, B.B. Straumal, S.G. Protasova, A.S. Gornakova, P. Zięba and T. Czeppe: JETP Lett. **96** (2012) 380–384.
165) O.A. Kogtenkova, P. Zieba, T. Czeppe, L. Lityn'ska-Dobrzynska, B.B. Straumal and A.N. Nekrasov: Bull. Russ. Acad. Sci., Physics **77** (2013) 1386–1390.
166) K. Higashi, T.G. Nieh, M. Mabuchi and J. Wadsworth: Scr. Metall. Mater. **32** (1995) 1079–1084.
167) Y. Takayama, T. Tozawa and H. Kato: Acta Mater. **47** (1999) 1263–1270.
168) H. Iwasaki, T. Mori, M. Mabuchi and K. Higashi: Acta Mater. **46** (1998) 6351–6360.
169) B. Baudelet, M.C. Dang and F. Bordeaux: Scr. Metall. Mater. **26** (1992) 573–578.
170) M. Mabuchi, K. Higashi, T. Imai and K. Kubo: Scr. Metall. **25** (1991) 1675–1680.
171) B.B. Straumal, A.A. Mazilkin, S.G. Protasova, S.V. Dobatkin, A.O. Rodin, B. Baretzky, D. Goll and G. Schütz: Mater. Sci. Eng. A **503** (2009) 185–189.
172) B.B. Straumal, A.O. Rodin, A.L. Petelin, B. Baretzky, S.G. Protasova, S.V. Dobatkin, J. Dutta Majumdar and I. Manna: Def. Diff. Forum **309–310** (2011) 51–62.
173) B.B. Straumal, S.V. Dobatkin, A.O. Rodin, S.G. Protasova, A.A. Mazilkin, D. Goll and B. Baretzky: Adv. Eng. Mater. **13** (2011) 463–469.
174) Yu. Ivanisenko, X. Sauvage, A. Mazilkin, A. Kilmametov, J.A. Beach and B.B. Straumal: Adv. Eng. Mater. **20** (2018) 1800443.
175) B. Straumal, R. Valiev, O. Kogtenkova, P. Zieba, T. Czeppe, E. Bielanska and M. Faryna: Acta Mater. **56** (2008) 6123–6131.
176) R.Z. Valiev, M.Yu. Murashkin and B.B. Straumal: Mater. Sci. Forum **633–634** (2009) 321–332.
177) R.Z. Valiev, M.Y. Murashkin, A. Kilmametov, B.B. Straumal, N.Q. Chinh and T.G. Langdon: J. Mater. Sci. **45** (2010) 4718–4724.
178) N.Q. Chinh, T. Csanádi, J. Gubicza, R.Z. Valiev, B.B. Straumal and T.G. Langdon: Mater. Sci. Forum **667–669** (2011) 677–682.
179) O.A. Kogtenkova, A.A. Mazilkin, B.B. Straumal, G.E. Abrosimova, P. Zięba, T. Czeppe, B. Baretzky and R.Z. Valiev: J. Mater. Sci. **48** (2013) 4758–4765.
180) B.B. Straumal, X. Sauvage, B. Baretzky, A.A. Mazilkin and R.Z. Valiev: Scr. Mater. **70** (2014) 59–62.
181) N.Q. Chinh, R.Z. Valiev, X. Sauvage, G. Varga, K. Havancsák, M. Kawasaki, B.B. Straumal and T.G. Langdon: Adv. Eng. Mater. **16** (2014) 1000–1009.
182) B.B. Straumal, A.A. Mazilkin, X. Sauvage, R.Z. Valiev, A.B. Straumal and A.M. Gusak: Russ. J. Non-Ferr. Metals **56** (2015) 44–51.
183) N.Q. Chinh, T. Csanádi, T. Győri, R.Z. Valiev, B.B. Straumal, M. Kawasaki and T.G. Langdon: Mater. Sci. Eng. A **543** (2012) 117–120.